

Climate Change Impacts on Jordan River Flow: Downscaling Application from a Regional Climate Model

RANA SAMUELS

Department of Geophysics and Planetary Sciences, Faculty of Exact Sciences, Tel Aviv University, Tel Aviv, Israel

ALON RIMMER

Yigal Allon Kinneret Limnological Laboratory, Israel Oceanographic and Limnological Research Ltd., Migdal, Israel

ANDREAS HARTMANN

Institute of Hydrology, Freiburg University, Freiburg, Germany

SIMON KRICHAK AND PINHAS ALPERT

Department of Geophysics and Planetary Sciences, Faculty of Exact Sciences, Tel Aviv University, Tel Aviv, Israel

(Manuscript received 20 May 2009, in final form 15 February 2010)

ABSTRACT

The integration of climate change projections into hydrological and other response models used for water resource planning and management is challenging given the varying spatial resolutions of the different models. In general, climate models are generated at spatial ranges of hundreds of kilometers, while hydrological models are generally watershed specific and based on input at the station or local level. This paper focuses on techniques applied to downscale large-scale climate model simulations to the spatial scale required by local response models (hydrological, agricultural, soil). Specifically, results were extracted from a regional climate model (RegCM) simulation focused on the Middle East, which was downscaled to a scale appropriate for input into a local watershed model [the Hydrological Model for Karst Environment (HYMKE)] calibrated for the upper Jordan River catchment. With this application, the authors evaluated the effect of future climate change on the amount and form of precipitation (rain or snow) and its effect on streamflow in the Jordan River and its tributaries—the major water resources in the region. They found that the expected changes in the form of precipitation are nearly insignificant in terms of changing the timing of streamflow. Additionally, the results suggest a future increase in evaporation and decrease in average annual rainfall, supporting expected changes based on global models in this region.

1. Introduction

Climate change is expected to have a negative effect on water resources and freshwater ecosystems in all regions of the world (Parry et al. 2007). Currently, the leading tools available for projecting future conditions of transient atmospheric circulation variables that are an effect of unseen CO₂ levels are global circulation models (GCMs). These models are based on physical equations

appropriate at spatial ranges of hundreds of kilometers. While they are obviously not perfect records of reality, the ability of GCMs to modify their forcings make them a useful tool for connecting anthropogenic emissions and effects on precipitation and evaporation at large scales (Déqué 2007). Although hydrological modules (precipitation, evaporation, land use) are also used within the GCMs, they are less reliable for analysis of surface and groundwater water balances in local river basins. The leading tools for these purposes are usually hydrological and agricultural models, used to support water policy and management decisions. These models are often valid for a particular watershed—geographically much smaller in size than the climate model—and usually calibrated with

Corresponding author address: Rana Samuels, Department of Geophysics and Planetary Sciences, Tel Aviv University, Tel Aviv 69978, Israel.
E-mail: ranas@post.tau.ac.il

local historical trends of streamflow or groundwater flow. Hydrological models by themselves cannot forecast future climate changes. The challenge then is to optimally combine the climate and hydrological models such that future forecasts of local changes and trends of natural water availability will be as reliable as possible.

The most common methods for transferring GCM output to variables at the local river basin scale include (i) delta change/ratio methods, which look at the percent (or amount) of change from present to future conditions; (ii) dynamical downscaling, using regional circulation models (RCMs) driven by GCMs; and (iii) statistical downscaling. Vicuna and Dracup (2007) surveyed 60 studies completed over the past two decades, focusing on the effects of climate change on water resources in California and applying various downscaling techniques. They conclude that the choices of which GCM and statistical method are used are key components for reliable future scenarios. In the past, statistical downscaling of rainfall using linear methodologies has been applied in Korea (Kim et al. 2004), over Turkey (Tath et al. 2004), and in Europe in the spring (Lloyd-Hughes and Saunders 2002). Classification methods such as hidden Markov models have been used in Ceara, Brazil (Robertson et al. 2004); the Rhine basin (Buishand and Brandsma 2001), Spain (Díez et al. 2005); and Israel (Samuels 2008). Bias-correction methods have been used to downscale daily precipitation and temperature in France (Déqué 2007) and Israel (Alpert et al. 2008). Different techniques can be chosen based on the research question being pursued.

In this paper, we present skillful methods for applying results from a dynamically downscaled regional climate model (RegCM) simulation focused specifically on the Middle East (Fig. 1a) to drive a local watershed model [Hydrological Model for Karst Environment (HYMKE); Rimmer and Salingar 2006]. In this way we can examine the effects of climate change on local water resources. The results of the RegCM driven by the German ECHAM5 GCM have recently been published (Krichak et al. 2007; Krichak et al. 2009) and here we provide a first prediction estimate for expected changes on streamflow in the region. Since the greatest uncertainty in climate change studies is typically the global model providing boundary conditions (e.g., Fowler and Ekström 2009), using an ensemble of global models is preferable to improve skill (see, e.g., Pierce et al. 2009). The results presented are limited to a single potential future projection, and they may not be representative of a model consensus. Currently, model runs using a different driving GCM have been undertaken in an attempt to begin addressing this uncertainty. Given these limitations, the results should be seen as a first

approximation used to test the ability of the approach and its sensitivity to changes in climate parameters in the vulnerable areas of the eastern Mediterranean (EM) and the Middle East. The approach should be improved and validated based on results from additional climate models. However, for now, the methodology can provide important information for water policy and planning.

This study specifically focuses on the important meteorological variables for precipitation and evaporation modeling and presents results for daily recharge of the three main sources of the Jordan River—Dan, Hermon (also known as Banyas), and Snir (also known as Hatzbani) tributaries—under climate change conditions for near-future (2010–35) and far-future (2036–60) time slices. While bias correction applied to precipitation is well documented, here we present a daily approach for calculating potential evaporation (PE) using meteorological parameters extracted directly from a RegCM. Additionally, while the results of the model presented here are specific to the region, the techniques used can potentially be applied to any RegCM to create precipitation time series and derive local PE data for use in a multitude of hydrological, agricultural, or water management models.

2. Study area: The upper catchments of the Jordan River

The study area in this paper is the upper catchments of the Jordan River (UCJR; Fig. 1b) with an area of $\sim 1700 \text{ km}^2$: $\sim 920 \text{ km}^2$ is in Israel and the rest is in Syria and Lebanon. These catchments are the major water source within the Lake Kinneret watershed, located in the northern part of the Jordan Rift Valley (northern Israel; Fig. 1a). Lake Kinneret contributes $\sim 30\%$ of the Israeli water consumption. The lake is heavily deployed through the Israeli National Water Carrier (NWC), the national water supply system that takes water from the lake and distributes it to other parts of the country. The average area of the lake surface is 166 km^2 , the average volume is 4100 Mm^3 , and the average annual inflows of natural sources (not including water diversion from the Yarmuk River) is $\sim 640 \text{ Mm}^3$. An average of 230 Mm^3 evaporate every year, so that the average annual volume of natural available water is $\sim 410 \text{ Mm}^3$. The renewal period of the lake is ~ 10 years.

The UCJR region includes four different hydrological units: (i) the Jurassic karst region of Mount Hermon, (ii) the basalt plateau of the Golan Heights, (iii) the eastern Galilee Mountains, and (iv) the flat alluvial Hula Valley. An average of $486 \times 10^6 \text{ m}^3$ of water is contributed annually (1969–2006) to the UCJR through the karstic

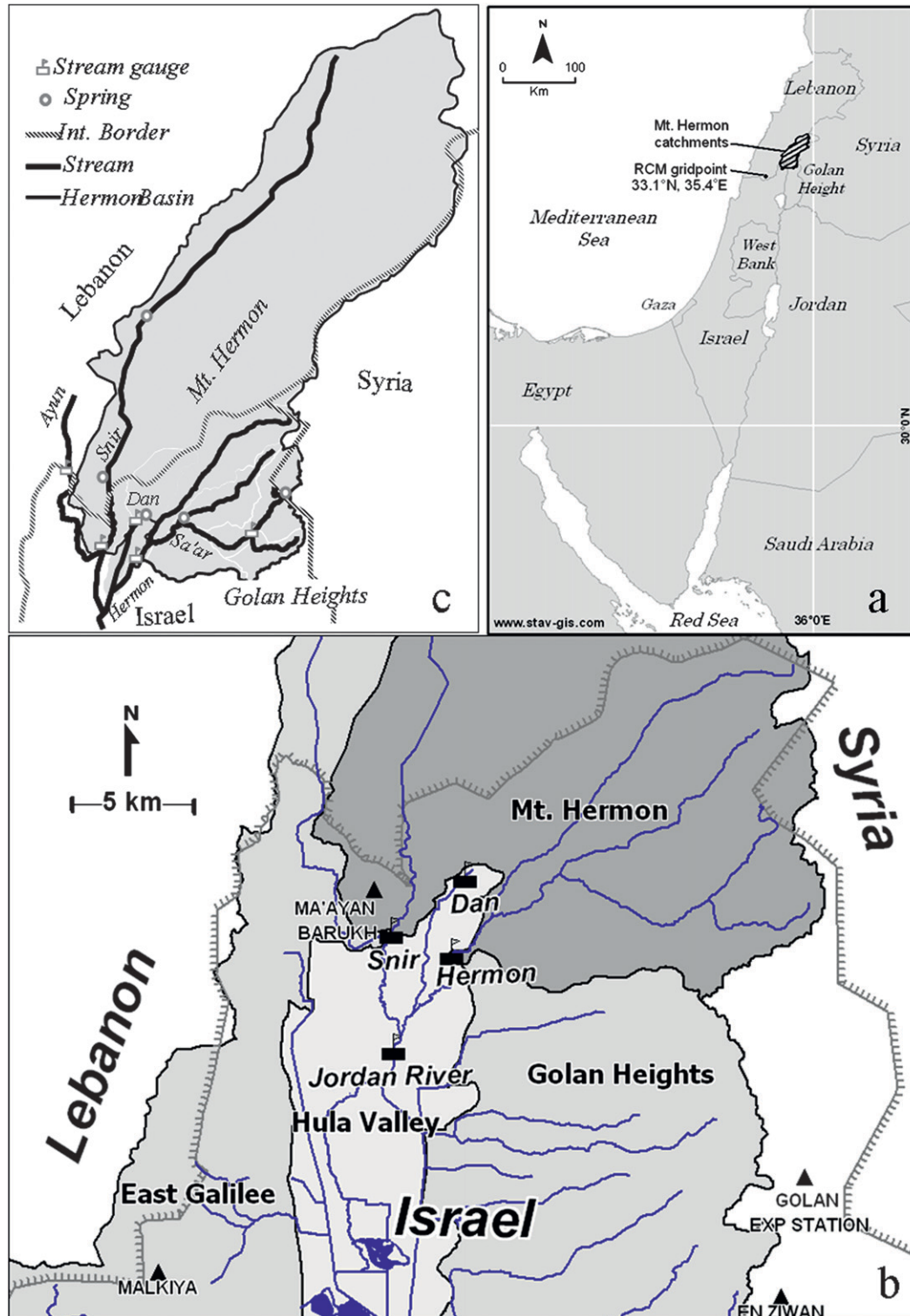


FIG. 1. (a) Orientation map of the EM with the locations of Mount Hermon catchments and the RegCM grid point (33.1°N, 35.4°E). (b) The four units of the UCJR with the location of four precipitation rain gauges. (c) Mount Hermon catchments with the Dan, Hermon, and Snir streams.

springs and surface flow of the Mount Hermon region (Fig. 1c), an elongated 55-km-long and 25-km-wide anticline of mostly karstic limestone with summits of 2814 m. Only 7% of the range lies in Israel, while the rest is divided equally between Syria and Lebanon. The Hermon high regions (above 1000 m MSL) receive the most precipitation in Israel ($>1300 \text{ mm yr}^{-1}$), restricted to the wet season from October to April. On the basis of data from the years 2006–08 (3 yr), the temperature gradient from the Hula Valley (elevation of $\sim 70 \text{ m MSL}$) to the summit of Mount Hermon was calculated as $\sim -0.43^\circ\text{C } 100 \text{ m}^{-1}$. During the winter months (January–March), the temperature on the highest parts of the mountain ($>1400 \text{ m}$) often reduced to below 0°C , and precipitation is mainly in the form of snow. Rainfall and snowmelt of Mount Hermon recharge the main tributaries of the upper catchments of the Jordan River (Fig. 1c): (i) Dan ($255 \times 10^6 \text{ m}^3$ annually), (ii) Snir ($118 \times 10^6 \text{ m}^3$), and (iii) Hermon ($107 \times 10^6 \text{ m}^3$).

The expected effects of climate change in the eastern Mediterranean and Middle East regions in general and in the study area in particular are worrisome indeed. As opposed to some regions in the world, the multiple Intergovernmental Panel on Climate Change (IPCC) models are fairly consistent when it comes to the region of the Mediterranean, where annual precipitation and the number of rainy days are very likely to decrease and temperatures, especially those in the summer, are likely to increase. Potential evaporation is also likely to increase with a higher likelihood of extreme events, increasing the importance of skillfully predicting droughts and floods (Giorgi et al. 2004; Parry et al. 2007; Krichak et al. 2009; Kunstmann et al. 2007).

3. Model descriptions

There are two physical models used in the research: (i) the RegCM3 and (ii) the HYMKE. This section describes general aspects of the two models, while the next section describes the techniques used to reconcile the different spatial scales of the models.

a. The RegCM

The RegCM chosen is the Abdus Salam International Centre for Theoretical Physics (ICTP) RegCM3 model driven from the lateral boundaries by the results of ECHAM5–Max Planck Institute Ocean Model 1 (MPI-OM1; Roeckner et al. 2003). A transient climate simulation from 1960 to 2060 under Special Report on Emissions Scenarios (SRES) A1B, where a balance between fossil fuel and other energy sources is assumed, is used. Details about the model run can be found in Krichak et al.

(2009). We used RegCM3, a third-generation model (Pal et al. 2007) of the ICTP with 50-km horizontal resolution and 14 vertical sigma levels, model top at 80 hPa, and five levels located below $\sim 1500 \text{ m}$. The model domain (Krichak et al. 2009) including the southern part of Europe, eastern part of the Mediterranean region and the Middle East as well as the physics options chosen [radiation (Kiehl et al. 1996); land surface model (Dickinson et al. 1993; Gao et al. 2006); planetary boundary layer (Holtslag et al. 1990); cumulus parameterization (Fritsch and Chappell 1980; Grell 1993); ocean flux parameterization (Zeng et al. 1998), lateral boundary treatment (Davies and Turner 1977); and cumulus parameterization according to Grell (1993) with Arakawa and Schubert (1974) closure; for references and further details, see Pal et al. (2007)] were selected according to results of earlier evaluations (Krichak et al. 2007). Also in the RegCM3 run, the greenhouse gas (GHG) concentrations varied according to the A1B scenario.

When compared with the other IPCC GCM models, the ECHAM model used to drive the RegCM3 shows a slower drying than most of the models from the 2020–40 period but catches up in the later decades (2040–60 and 2060–80). This trend can be seen in our model results here as the earlier 2010–35 period have little change with much of the decrease in precipitation taking place in the 2035–60 period (see section 5).

Table 1 shows a comparison of seasonal daily data (October–March) between the RegCM3 (50-km horizontal resolution–14 vertical levels) and observed data from the Golan Experimental Station (GES) for the years 1975–2005. The results indicate that the specific run of this model is able to capture intraseasonal statistics, such as the number of wet days, as well as persistence indicators, such as wet spells and dry spells, and transition probabilities between wet days and dry days effectively across the different quantiles (2.5%–97.5%). Similar comparisons were seen at other stations in the area. This validation of the model is important, because in addition to the total amount of rainfall, it is the persistence or absence of rainfall events that plays a major role in determining streamflow, specifically peak events. A more comprehensive comparison of the RegCM3 with other climate models and at additional stations is currently underway.

b. The HYMKE

The HYMKE (Rimmer and Salingar 2006) used in this study receives daily precipitation and PE time series as input. Prediction of the effect of such meteorological changes on the streamflow and river systems is not trivial. For such analysis, established and well-calibrated mechanisms for groundwater and streamflow recharge is

TABLE 1. Comparison of intraseasonal results from the RegCM3 with data from the GES for different quantiles. Results are calculated from the rainy season between October and April during the years 1975–2005. Number of wet days, number of 7-day dry spells, and number of 3-day wet spells are shown along with the probability of having a wet day following a wet day and a dry day following a dry day.

(%)	Number of wet days		7-day dry spell		3-day wet spell		Wet–wet P (%)		Dry–dry P (%)	
	GES	RegCM3	GES	RegCM3	GES	RegCM3	GES	RegCM3	GES	RegCM3
2.50	35	42	7.3	7.3	6.0	4.3	0.09	0.10	0.47	0.47
25	51	55	10.0	9.0	8.8	8.0	0.14	0.14	0.53	0.55
50	63	61	12.0	11.0	12.0	10.0	0.18	0.16	0.60	0.59
75	75	71	15.0	13.0	14.3	13.3	0.23	0.21	0.67	0.63
97.50	87	84	19.4	17.4	18.7	18.7	0.29	0.26	0.76	0.72

needed. A first attempt to look at climate change on the Jordan River was done using a noncalibrated, distributed hydrological model that was not able to account for the karstic environment and corresponding preferential flow paths, which are typical of the Mount Hermon region (Kunstmann et al. 2007). In the specific karst area of the Mount Hermon region, the location of different aquifers and the discharge area of the three main tributaries are unknown. Moreover, from the ratios of fast to base flow, it is clear that these recharge areas are not correlated with the size of the geographic surface water catchments. HYMKE is therefore based on the idea that the fast-flow component is correlated with the geographical catchment area, while the area of the groundwater aquifer is a parameter that should be calibrated against the separated, measured base flow. This aspect of karst hydrology was discussed in detail in previous papers (Rimmer and Salingar 2006; Rimmer 2009). The main equations in HYMKE are composed of five modules (Fig. 2): 1) the snow routine, 2) surface layer, 3) surface (“fast”) flow, 4) vadose zone, and 5) groundwater. Unlike the other parts of the model that were published by Rimmer and Salingar (2006), the snowmelt routine is new in the HYMKE structure. This module uses the precipitation and temperature data from the RegCM3 and analyzes it separately to produce snow and snowmelt in 56 discrete stripes of 50-m height, in elevation from 75 to 2825 m. It uses the approach of the standard Hydrologiska Byråns Vattenbalansavdelning (HBV) model after Bergström (1995). HBV is based on the degree-day temperature-index approach. With currently available temperature data, we calibrated the actual temperature gradient and evaluated the daily temperature of each elevation strip, so that the input to the snow routine is fairly accurate. However, because of the lack of measured snowmelt at the latitude of Mount Hermon, several parameters of the model could not be calibrated and were adopted from the literature on alpine climates (Hamilton et al. 2000; Moore 1993; Seibert 1997). Melting temperature was 0°C, the degree-day factor was set at 2 mm °C⁻¹ day⁻¹, the refreezing factor was set to 0.05,

and holding capacity of snow cover as fraction of total water equivalent was set to 0.1.

The daily amount of water in the surface layer (module 2) of each elevation is controlled by precipitation and snowmelt, actual evaporation (based on the input of daily PE), and downward seepage to the vadose zone. Upon saturation the surface layer generates both fast flow and downward preferential flow. The fast-flow component reaches the stream via the surface flow routine (module 3). The preferential flow bypasses the upper soil layer and enters directly into the vadose zone routine (module 4), therefore recharging the vadose zone with fast preferential flow component and “slow” Darcian outflow from the surface layer. The vadose zone routine is a linear reservoir that feeds the groundwater routine (module 5), which finally yields the base flow of the subsurface system. The accumulating output from the surface runoff (module 3) and the base flow (module 5) for each tributary results in the full natural flow. The sum of all three tributaries creates the flow in the main stream, the Jordan River.

Model calibration was carried out using daily discharges of the main UCJR tributaries, measured by the Israeli Hydrological Service. In the three measured flow time series, the base flow was separated from the fast flow and created six time series—two for each of the three tributaries. Baseflow separation technique was based on the Eckhardt (2005) method and verified for these tributaries by comparing the “separated” baseflow component to the direct measurements of spring discharge (Rimmer and Salingar 2006). Model calibration was performed by reconstruction of both the surface and base flows during a continuous period from 1 January 1986 to 30 September 2000, and then it was verified by applying the calibrated parameters to the periods 1 January 1970–31 December 1985 and 1 October 2000–30 September 2004. The calibration resulted in correlations of $R^2 = (0.60, 0.75)$ between the calculated and separated surface flows of the Snir and Hermon tributaries, respectively; correlations of $R^2 = (0.84, 0.89, 0.77)$ and Nash–Sutcliffe coefficient $NC = (0.71, 0.80, 0.21)$

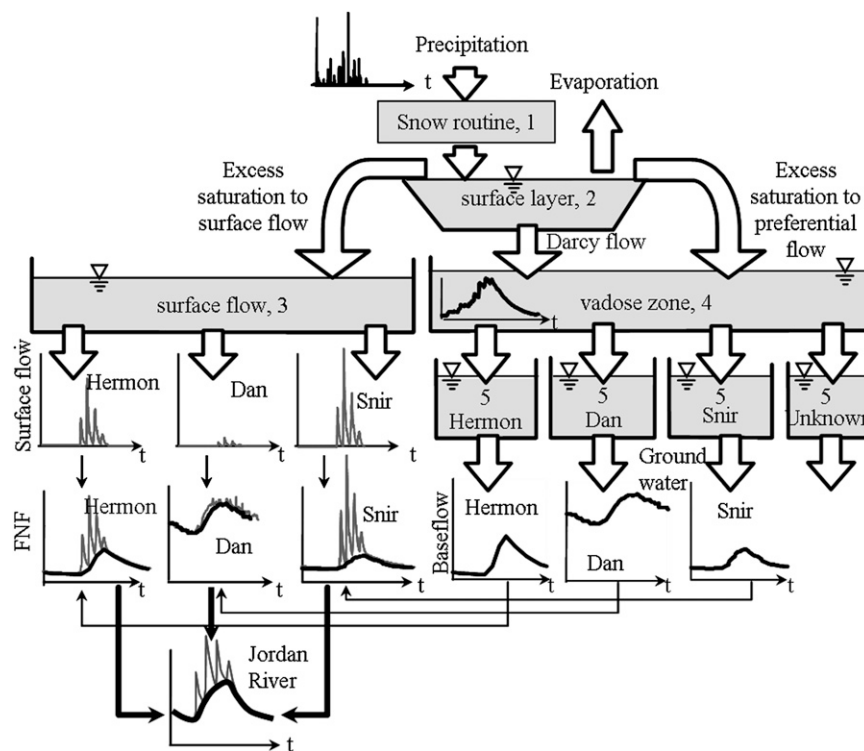


FIG. 2. Schematic description of the Mount Hermon conceptual hydrological model, consisting of five modules: 1) precipitation–snow routine; 2) surface layer; 3) surface flow as linear reservoir; 4) the vadose zone linear reservoir; and 5) four groundwater linear reservoirs representing main springs (see text). The calculated base flow and the surface flow components of each tributary result in their full natural flow, and the combined flow creates the Jordan River.

between the calculated and separated base flows of the Snir, Hermon, and Dan streams, respectively; and correlation of $R^2 = 0.94$ and $NC = 0.79$ between the calculated and measured flows of the Jordan River (Fig. 3). The relatively low NC for the Dan base flow is because its flow is less sensitive to extremely dry or wet seasons and therefore more difficult to model for such conditions. While this model has previously been used to evaluate hypothetical scenarios and changes in precipitation (Samuels et al. 2009), this is the first time that actual climate model results are used as future input.

4. Methodology

There are three main components in this study. The first component is the comparison of raw data extracted from the RegCM3 with historical measured data. The second component, based on this analysis, is that the RegCM3 output was transformed into appropriately scaled precipitation and PE time series necessary for input into the hydrological model. Lastly, the new time series were used as input into the hydrological model

to determine the effect of future climate change on streamflow.

Initial evaluation of data extracted from the RegCM3 was performed by comparing modeled to measured data from a historical 25-yr period, 1980–2004.¹ This period was chosen because it is the last 25-yr period for which a complete dataset is available. Though the accepted length of a “climate period” is 30 yr, in this study we chose a 25-yr period. The reason for this is that we wanted to examine two sets of future data: near future and far future. However, the RegCM3 data are from 1960 to 2060, and since it is desirable that future periods do not overlap, we divided the RegCM future data into future periods of 25 yr each: (i) near future, 2011–35; and (ii) far future, 2036–60. Therefore, for the historical period, a period of 25 yr was also chosen. A comparison of the cumulative distribution functions from the 25-yr period (1980–2004) and the 30-yr period (1975–2004) showed

¹ Years are defined as hydrological years, October–September. The year refers to the year in January.

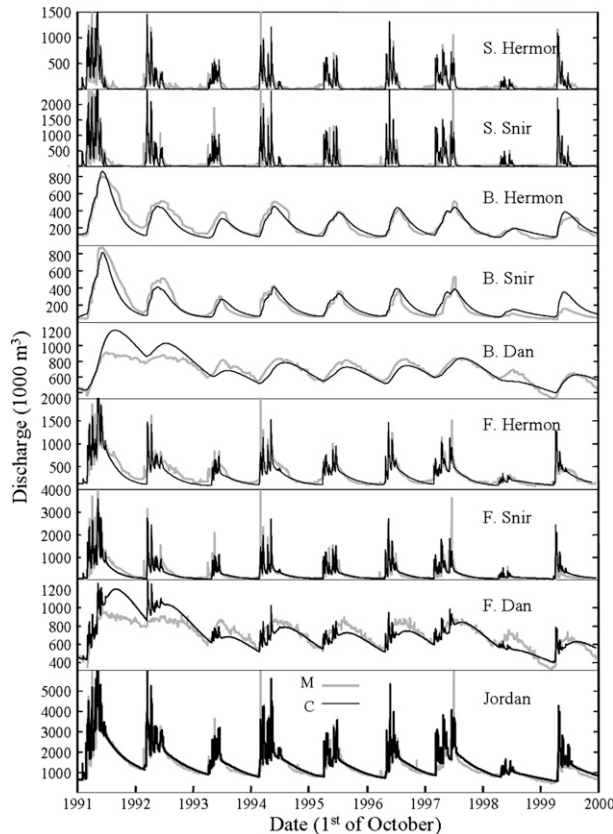


FIG. 3. Calculated (C) vs measured (M) for the years 1991–2000: surface flow of the Hermon and Snir streams (S), base flow of the three main tributaries (B), full natural flow of the tributaries (F), and the cumulative flow of the Jordan River (Jordan).

that the bias-correction technique was not sensitive to the 5-yr difference.

The rest of this section describes the methods used to generate the precipitation and PE time series from the output of the RegCM3. These methods include two procedures: (i) a bias-correction method used for down-scaling the rainfall time series (section 4a) and (ii) an estimation of RegCM3 based daily PE using the Penman–Monteith equation (section 4b).

a. Bias correction of the rainfall time series

The amount of precipitation on Mount Hermon itself was not measured systematically before 2006 because of the difficulties in maintaining meteorological stations at altitudes above 2000 m MSL (Gil'ad and Bonne 1990). Therefore, previous applications of HYMKE used default input of rainfall time series based on long-term (1970–2005) daily precipitation data from four stations, located in Ma'ayan Baroukh, Malkiya, GES, and Ein Ziwan (Fig. 1c). Data were supplied by the Israeli Meteorological Service. These four stations were chosen

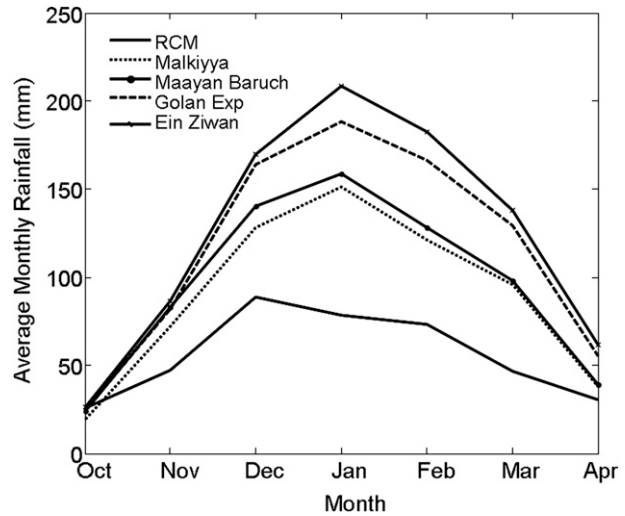


FIG. 4. Monthly comparison of data for precipitation stations and for the raw RegCM3 output.

because they represent various elevations in the northern UCJR. The rainfall series were compiled and corrected to prevent missing and erroneous values (less than 1%) using linear regression with neighboring rain gauges. The modeled precipitation from the RegCM3 was compared with the measured rain from these stations over the winter season. The output was extracted from the grid point closest to the rain gauges. Analysis of the eight surrounding grid points indicated that their use did not change the results after the bias correction. The intensity of modeled rainfall is much lower than the measured rainfall (Fig. 4). This can be explained by the fact that the 50-km spatial scale is too coarse to resolve orographic and convective processes. In addition, there is a seasonal bias with the RegCM3 data peaking in December as opposed to January in the station data. Given these differences in rainfall intensity and distribution, a bias-correction technique based on statistical correction of observed and modeled values was used to down-scale the RegCM3 precipitation data to the station level. This technique has been used on rainfall and temperature data in France (Déqué 2007) and Israel (Alpert et al. 2008) and has been shown to capture seasonal trends as well as extreme values. However, in this case, given the seasonal bias of the RegCM3, the technique was applied to each month separately. In this bias-correction procedure, for each month, the daily values from both the observed data and modeled data for the historical period are ordered sequentially. These two time series are then divided into percentiles and the mean for each percentile is calculated. The bias-correction factor (bcf) for each percentile i for each month m is calculated by subtracting the mean of the modeled data y from the mean of the

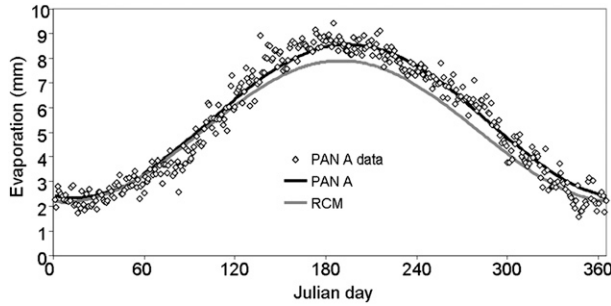


FIG. 5. Daily PE in the UCJR (mm). Pan A data: average daily PE from 30 yr and three stations—Dafna (150 m), Ayelet HaShahar (180 m), and Gamla (380 m). Pan A = Annual PE trend determined by Eq. (1) and Pan A data. RCM = Annual PE trend determined by Eq. (1) and RegCM3 data for 1980–2005.

observed data x such that $bcf_{im} = (\bar{x}_{im} - \bar{y}_{im})$. This correction factor is then applied to all the daily values in the modeled time series based on the appropriate percentile and month. This new bias corrected time series is then used as input into the hydrological model.

An additional variable needed for the snow routine was the daily average temperature. Given the good approximation of this variable by the RegCM3 for the years 1980–2004 (see Fig. 6), the temperature from the RegCM were applied to the snow routine in HYMKE without any modification, and the temperature gradient was used to define the attributed temperature to each elevation stripe.

b. Potential evaporation

Originally, in the default run of HYMKE (Rimmer and Salingar 2006), PE estimations were based on long-term (1970–2000) daily measurements of Pan A evaporation (Ponce 1989). Measurements from three locations (Gamla at an elevation of 380 m, Ayelet HaShahar at 180 m, and Dafna at 150 m MSL; Fig. 5) were available. Mean seasonal Pan evaporation averages were used to fit a seasonal Pan A evaporation trend (PE_A , mm), determined by

$$PE_A = b_E \{1 + a_E \sin[\lambda_E (JD + \omega_E)]\}. \quad (1)$$

Here JD is the day of the year, a_E and b_E are constants that determine the amplitude in mm, λ_E is the angular frequency (rad), and ω_E is the phase shift. However, for a future scenario under an evolving climate, PE_A , as proxy measures for PE, is not valid. Also, changing the future PE by multiplying past data by a factor (e.g., Rimmer 2009; Viney and Sivapalan 1996) does not take into account the RegCM3 results. Moreover, the RegCM3 provides daily output of actual evaporation calculated using a standard surface drag coefficient formulation based on surface-layer similarity theory (Elguindi et al. 2007).

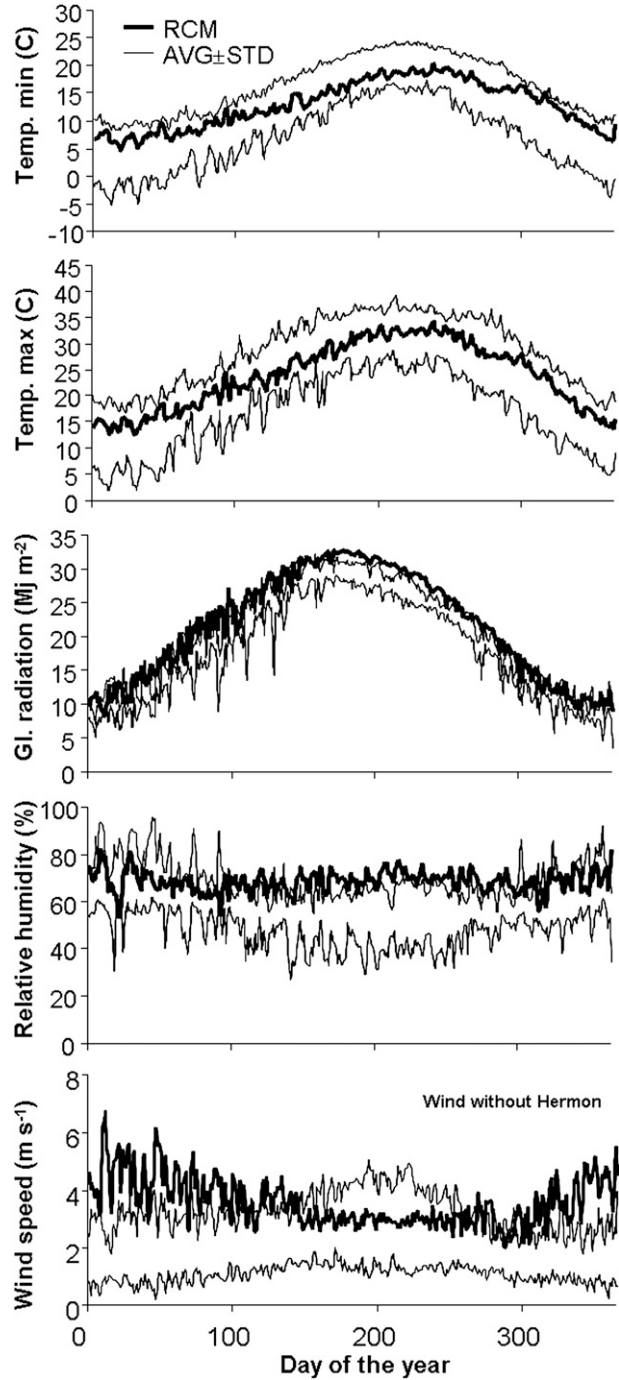


FIG. 6. Daily averages of RegCM3 results (1980–2004) for (top to bottom) minimal and maximal daily temperatures, global radiation, relative humidity, and wind speed, compared to the average ± 1 standard deviation of the same variables, measured at five meteorological stations in the UCJR (Hermon, Tabgha, GES, Kadesh, UGFCEs). Note that measured wind from the Mount Hermon station is not included.

TABLE 2. Description of five standard meteorological stations in the UCJR. IOLR refers to Israel Oceanographic and Limnological Research Ltd.

Station	Operator/data provider	Air temperature (°C)	Relative humidity (%)	Global radiation ($W m^{-2}$)	Wind speed ($m s^{-1}$)
1. Tabgha: Data available since 1996, onshore Lake Kinneret; elevation: -210 MSL; coordinates: 32°51.95' N, 35°33.01'E	Yigal Allon Kinneret Limnological Laboratory, IOLR	R. M. Young 43372C relative humidity and temperature probe at 5 m above water level	Kipp & Zonen DELFT BV shortwave radiometer CM11, at 5 m above water level	R. M. Young wind monitor MA-05106, at -204.85 m above sea level	
2. Hermon: Data available since December 2006 on top of Mount Hermon; elevation: 2082 m MSL; coordinates 33°18.499'N, 35°47.135'E	Yigal Allon Kinneret Limnological Laboratory, IOLR	Rotronic MP10TA air temperature and relative humidity, RH/T, installed 2.8 m above surface Operating range: -40°C to +60°C, accuracy of $\pm 0.2^\circ C$ Accuracy of the humidity sensor is $\pm 1.5\%$ with reaction time of 0.25 s	Kipp and Zonen CM3 pyranometer, installed 3.1 m above surface, reaction time (85%) of 18 s, and accuracy of $\pm 2.5\%$	Gill Instruments WindObserver II anemometer (Gill instruments), installed 6 m above surface	
3. GES: Data available since 2000, on the Golan Height; elevation: 960 m MSL; coordinates: 33°07'N, 35°48' E	Israeli Meteorological Service	Rotronic air temperature and relative humidity MP10TA model, RH/T, installed 2.0 m above surface	Kipp & Zonen CM11 pyranometer	R. M. Young 05103 wind monitor installed 8.0 m above surface	
4. Kadesh: Data available since 1995, on the eastern Galilee Mountains; elevation: 410 m MSL; coordinates: 33°11'N, 35°32'E	Agrometeorology Services of the Upper Galilee Regional Council	Campbell Scientific CS500 temperature and relative humidity probe, installed 2.0 m above surface	Campbell Scientific LI200X pyranometer	R. M. Young 03001 Wind Sentry Set, installed 2.0 m above surface	
5. UGFCEs: Data available since 1991 in the Hula Valley; elevation: 80 ASL; coordinates: 33°11'N, 35°35'E	Agrometeorology Services of the Upper Galilee Regional Council	Campbell Scientific CS500 temperature and relative humidity probe, installed 2.0 m above surface	Campbell Scientific LI200X pyranometer	R. M. Young 03001 Wind Sentry Set, installed 2.0 m above surface	

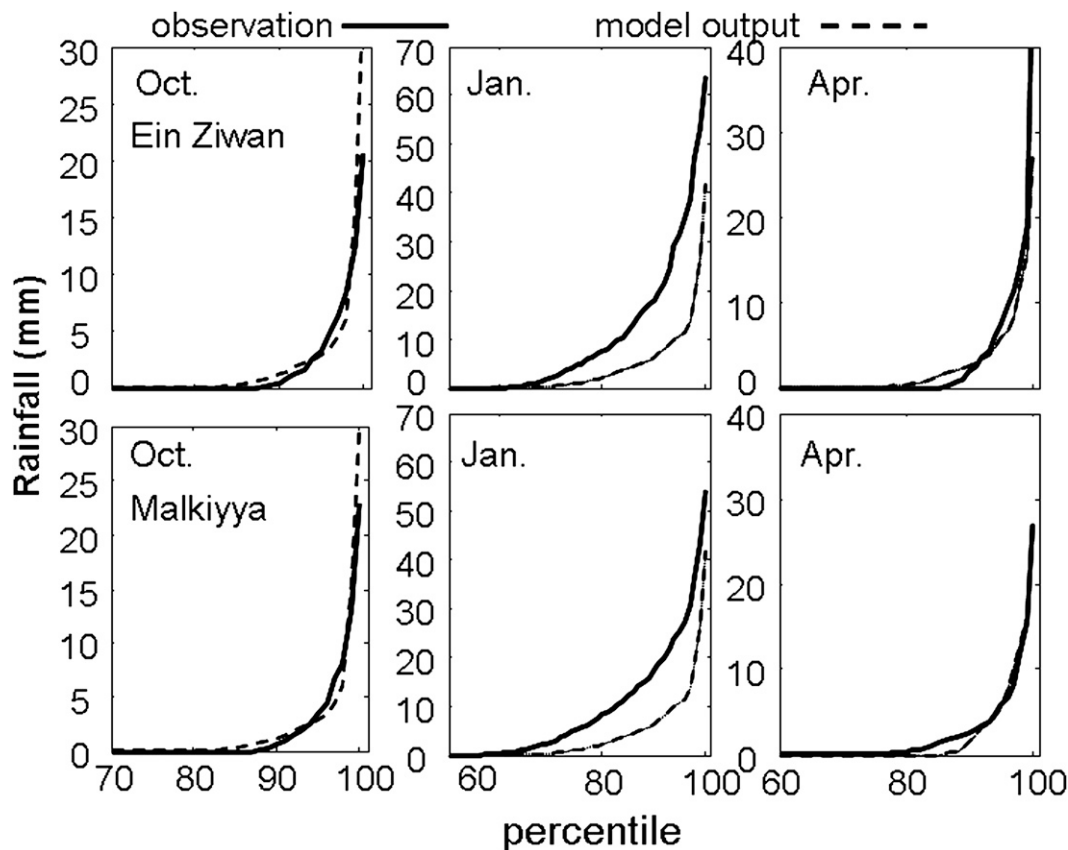


FIG. 7. Inverse CDF for precipitation (mm day^{-1} along the y axis) for October, January, and April based on observed values at two rainfall stations—(top) Ein Ziwan and (bottom) Malkiyya—and RegCM3 results from a grid point centered at 33.1°N , 35.4°E with a 50-km radius for the years 1980–2004 (25 yr), based on the percentiles (% along the x axis) of the daily values: observation (solid lines) vs model output (dashed lines).

However, in the selected grid point, the RegCM3 resulted in the annual average evapotranspiration of ~ 950 mm, while the annual average of representing rainfall on the Hermon catchment is only ~ 960 mm (this is an estimated average of the accumulated precipitation, taking into account the distribution of heights on Mount Hermon; see Rimmer and Salinger 2006). Therefore, using the direct evapotranspiration output from the large-scale RegCM3 for the local catchment is obviously not appropriate.

To address the problem of PE evaluation as input to the hydrological model, we applied a regulated procedure, through which we are able to identify the strengths and weaknesses in the climate model to know which of the results are more reliable and where we should expect some errors. First, we calculated the daily averages of RegCM3 results for the first period (years 1980–2004) of the following variables: minimal and maximal daily temperatures, global radiation, relative humidity, and wind speed. Then, these daily averages were compared with averages and confidence limits of measured meteorological

variables (Fig. 6) from five standard meteorological stations in the UCJR (see Table 2 for more details about these measurements). When we introduced the variables from the RegCM3 simulation into the well-known equation of Penman–Monteith (Allen et al. 1998; Valiantzas 2006), we found that the calculated PE (PE_{RCM}) was nearly similar to the results from the measured station data. Lastly, the PE_{RCM} annual trend was compared and scaled monthly to fit PE_{A} . This entire procedure resulted in a daily time series of PE_{RCM} solely based on the climate model. The results of this procedure, its limitations, and its application to future scenarios are discussed further in the next section.

5. Results

a. Downscaled parameters from the RegCM3

1) PRECIPITATION TIME SERIES

Precipitation time series from the RegCM3 were corrected for use in the hydrological model. A sampling of

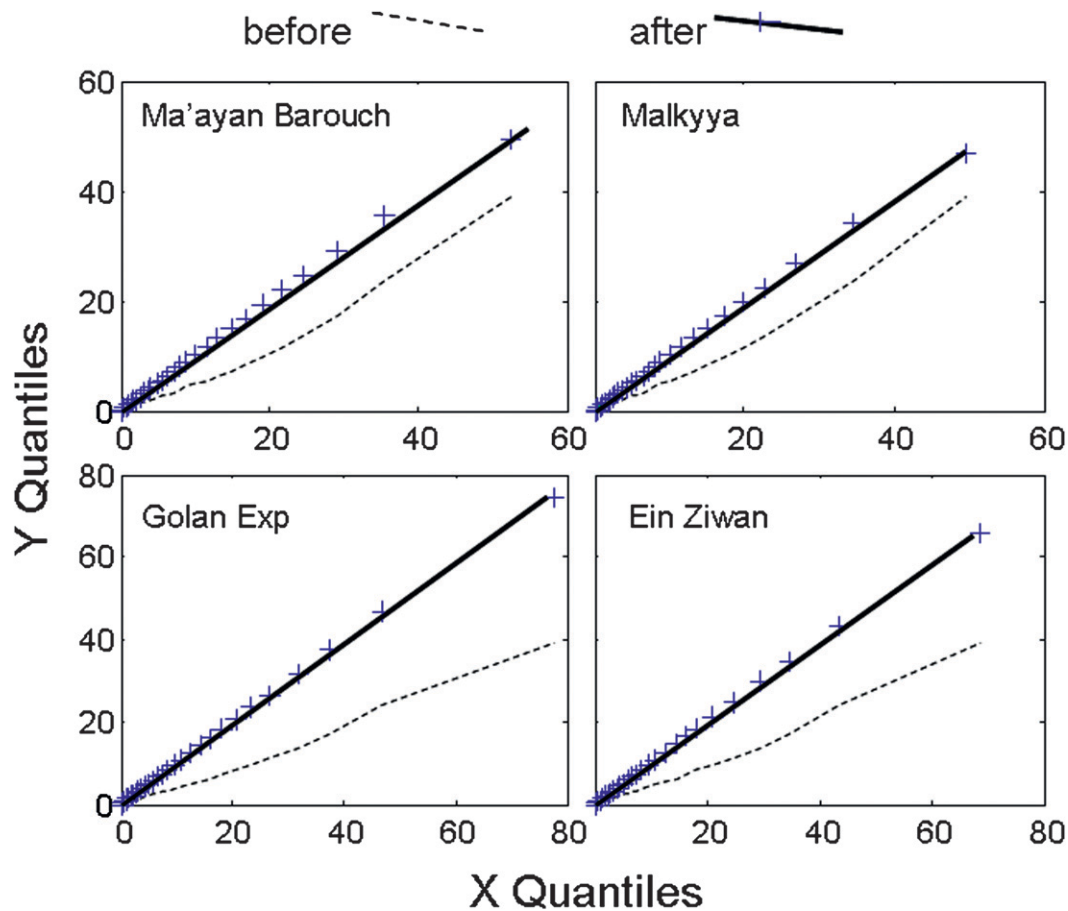


FIG. 8. Quantile–quantile plots of observed and model data before and after bias correction.

the inverse cumulative distribution functions (CDFs) used for the bias correction is shown in Fig. 7. The magnitude of the bias correction for each percentile for October, January, and April at Ein Ziwan and Malkiya for the 25-yr period of 1980–2004 is depicted. The correction necessary is larger both for months with higher rainfall (January as opposed to October or April) and for stations with higher rainfall (Ein Ziwan as opposed to Malkiya). The quantile–quantile plots (Fig. 8) show the fit of the RegCM3 data to the observed data before and after the bias correction for the whole season combined. The observed values correspond to the x axis and the model values to the y axis. Figure 9 summarizes the RegCM3 precipitation time series analysis for Ein Ziwan, from the typical daily values (Fig. 9a) to the control time series before and after the bias correction (Fig. 9b), and for the entire period (Fig. 9c). For the near future, we see that the mean and interannual variability stays fairly consistent with the recent past, while the far-future period is characterized by a decrease in rainfall. In terms of monthly distribution, Fig. 10 shows the average down-scaled monthly rainfall in the Hermon region for the

historical period as well as for the two future periods. While there is a slight increase in precipitation in the near-future period for October–January and March, there is a distinct decrease in the annual average of about 10% in the far-future period (2036–60) as compared to the historical period (1980–2004). These results indicate that the monthly bias correction is a robust technique to generate precipitation time series at the station level from the RegCM3 simulation.

2) POTENTIAL EVAPORATION CALCULATIONS

The stations we used (Table 2 and Fig. 6) are only ~ 50 km apart, but they represent varieties of climatic conditions in the UCJR. The two extreme meteorological stations are Mount Hermon (2080 m MSL) and Tabgha on the shore of Lake Kinneret (-210 m MSL). On Mount Hermon, the temperatures are $\sim 15^\circ$ lower; the global radiation is ~ 5 MJ (m) $^{-2}$ higher, especially during the summer; the relative humidity is $\sim 20\%$ lower, also during the summertime; and the wind is at least 2 times higher than in the Tabgha station. The RegCM3 results of the minimal and maximal temperatures (which

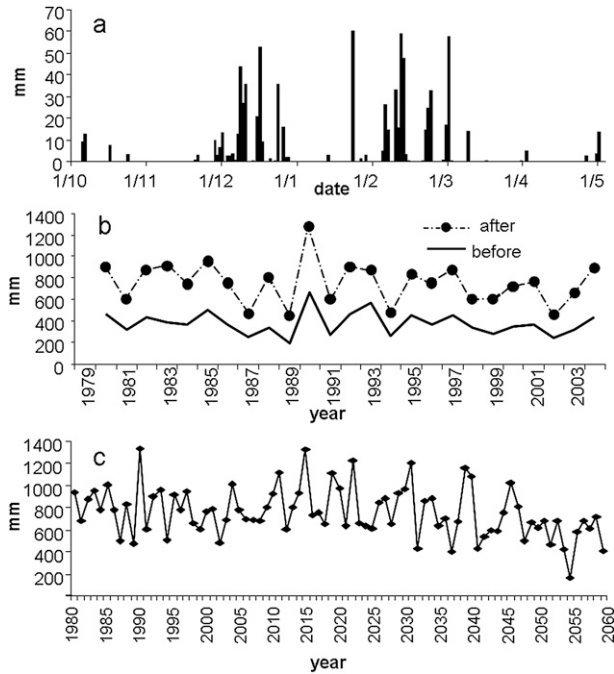


FIG. 9. Precipitation time series for Ein Ziwan station: (a) typical downscaled daily precipitation over a 7-month period; (b) annual precipitation from the RegCM before and after the bias-correction procedure (1979–2004); and (c) annual precipitation based on the downscaled results of the RegCM3.

represent an average of more than 50 km) usually fall between the confidence limit of the five measurement points. Note, however, that the RegCM3 global radiation is slightly higher than even the measured radiation on Mount Hermon, and the RegCM3 relative humidity is higher than the measured data, especially during the summer (even higher than the relative humidity in Tabgha station, onshore Lake Kinneret). A major difference was found between the calculated and measured wind pattern, which the RegCM3 overestimates during the winter and underestimates during the summer (the measured Mount Hermon wind was not included in the comparison in Fig. 6 because it currently has slightly more than one year of wind measurements). These differences are reflected well in the calculated PE_{RCM} , as shown in Fig. 11.

The PE_{RCM} results and the PE from five stations for 2008 (Fig. 11) are divided into the radiation component and the aerodynamic component, which together form the complete PE. These values are shown compared to the empirical seasonal PE curve, calculated from Pan A measurements. In the Kinneret, Upper Galilee Field Crops Experimental Station (UGFCES), and Kadesh stations, the radiation component is larger than the wind component, which is significantly reduced by the high relative humidity. On the Golan Heights (GES),

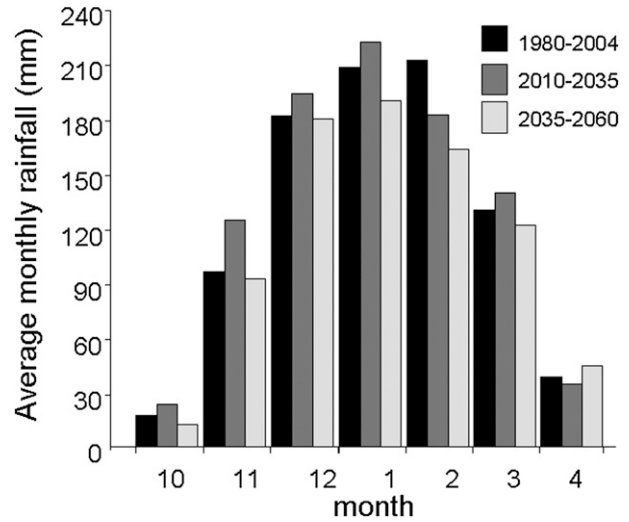


FIG. 10. The seasonal distribution of monthly precipitation on Mount Hermon (mm) for the three tested periods.

the wind component increase is due to stronger winds, while on Mount Hermon, the radiation component is relatively small because of the low temperatures; however, the aerodynamic component is fairly large because of low humidity and strong winds. The radiation component of PE_{RCM} seems to be higher than in the measured cases, clearly due to the higher solar radiation. On the other hand, the modeled aerodynamic component is smaller because of higher relative humidity and lower wind, especially during the summer. Analysis of this variety of meteorological data results in nearly similar annual trends of PE, mainly because the sum of the radiation component and the aerodynamic component are nearly similar. A detailed analysis of the specific components reveals that the RegCM3 data slightly overestimate radiation and underestimate wind speed; however, in the PE calculation, these biases cancel each other out.

The relatively weak winds and high humidity from the RegCM3 resulted in slightly reduced PE_{RCM} compared to the measured annual PE, especially during the summer month (see Fig. 5 as compared to the PE_A annual trend). To ensure that the statistical characteristics of the downscaled PE_{RCM} time series for the past years (1980–2004) are similar to those of the measured PE_A (both the measurements of Pan A evaporation and the calculated Penman–Monteith series), we scaled the input of the hydrological model (PE_S) using a monthly factor,

$$PE_S(j) = PE_{RCM} \times F_j;$$

$$F_j = 0.951 + 0.0167 \times j + 0.0031 \times (j - 6.5)^2;$$

$$j = 1, 2, \dots, 12. \quad (2)$$

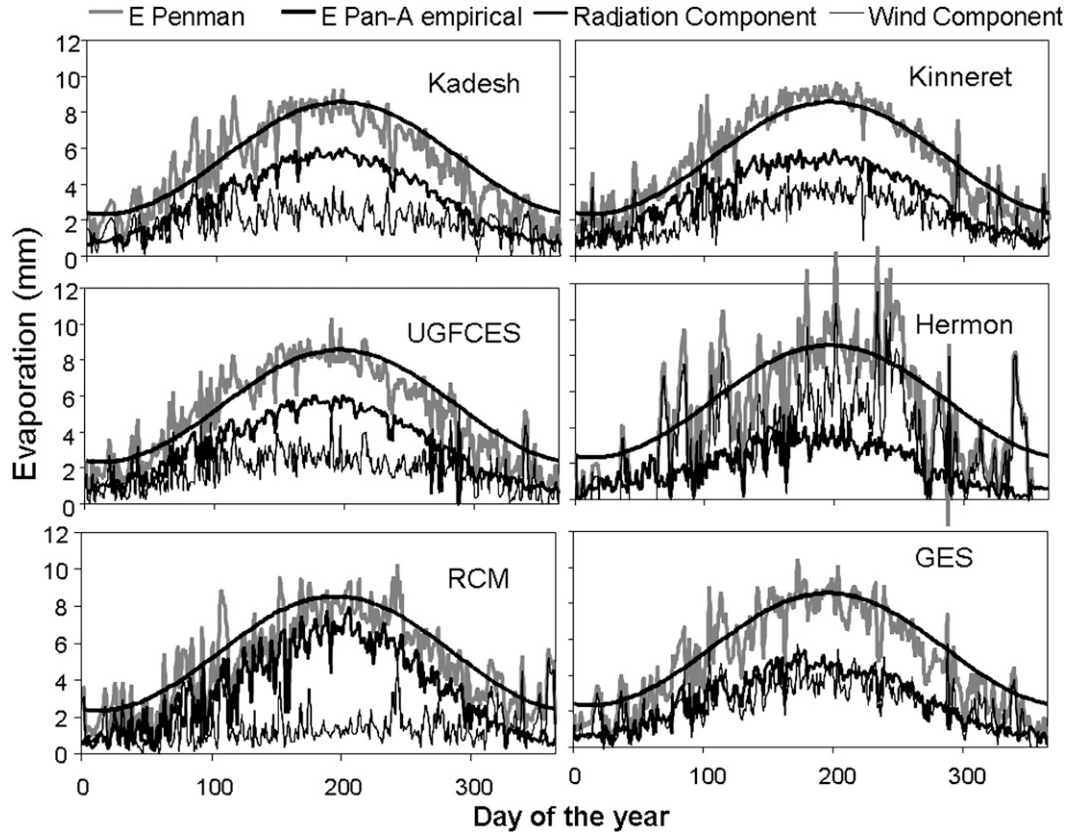


FIG. 11. Annual trend of average PE from Pan A measurements (heavy black line) compared with calculated Penman–Monteith values (gray line) and divided into the radiation and wind components for the RegCM3 data and five measurement locations (Hermon, Tabgha-Kinneret, GES, Kadesh, and UGFCEs).

The factor corrected the PE_{RCM} so that it would fit the PE_A annual trend. This correction factor was obviously used for the second and third periods as well (i.e., 2010–35, 2036–60). Figure 12 shows the average daily PE_S for the years 1980–2060 based on the meteorological data from the RegCM3. Similar to rainfall (Fig. 9c), the near-future period (2010–35) showed no increase in PE_S , while the far-future time slice (2036–60) was characterized by an average increase of 5%.

b. Rainfall and streamflow simulations

Application of the generated precipitation time series with HYMKE was carried out with a procedure nearly similar to what was described by Rimmer and Salinger (2006). A “representing” rainfall gauge of the entire Hermon region was defined and calculated based on the downscaled RegCM3 time series. A representing rainfall gauge of the entire Hermon region was defined as follows: The $\sim 783 \text{ km}^2$ region was divided into 56 strips of equal elevations from 75 to 2825 m with 50-m increments, and the area of each strip was calculated. Then, the daily measured (or modeled RegCM3)

precipitation of four rain gauges in various elevations—Ein Zivan, 948; GES, 960; Malkiya, 690; and Ma’ayan Barouch, 240 m—were used to calculate an average factor F of the daily rainfall. The factor was then used to calculate the daily, representing precipitation on each elevation stripe and on the entire watershed. The precipitation and temperature time series were used in the snow routine to calculate rainfall and snowmelt for each

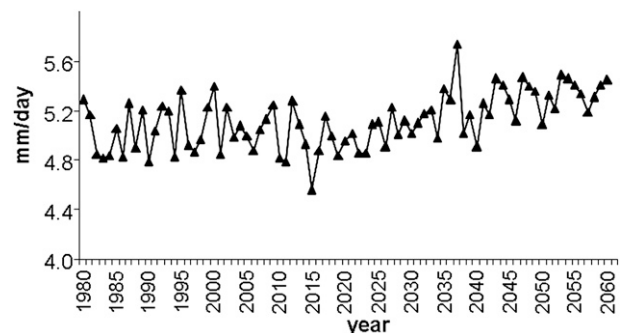


FIG. 12. Annual time series of PE (mm day^{-1}) based on the scaled results of the RegCM3 for the years 1980–2060.

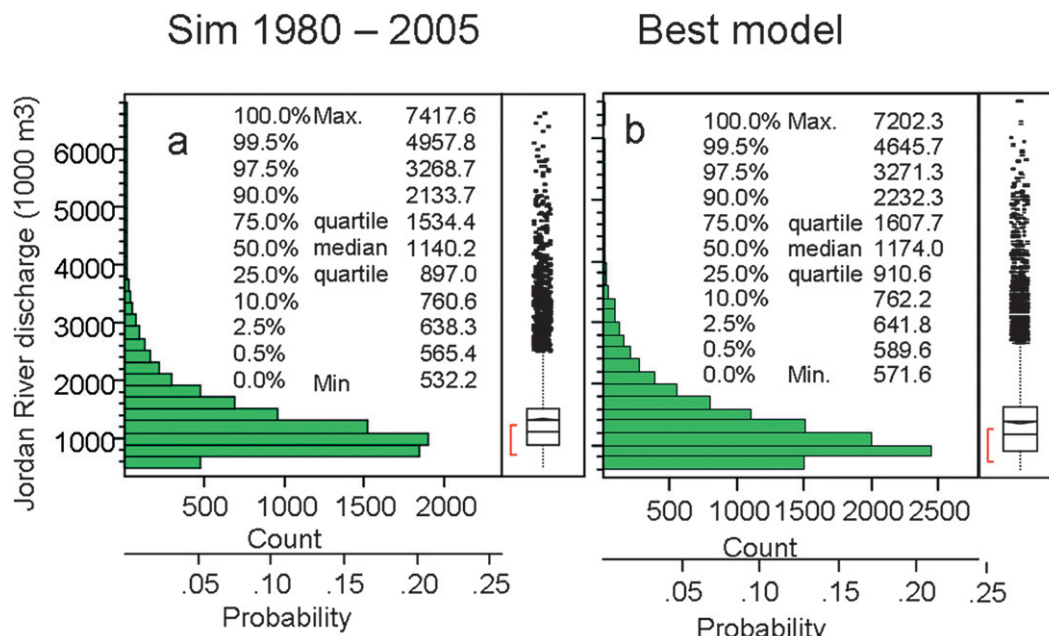


FIG. 13. Distribution of calculated full natural flow in the Jordan River: (a) simulated with RegCM3 input for the period 1980–2005 (validation) and (b) the best model results using the measured rainfall and EP_A data (original). The R^2 between probabilities is >0.99 .

elevation. Simultaneously, the daily PE was calculated with the application of the RegCM3 meteorological data. In each simulation, HYMKE created 12 time series: base flow, surface flow, and full natural flow for the Dan, Snir, and Hermon streams and the Jordan River.

1) VALIDATION OF THE COMBINED RAINFALL AND STREAMFLOW SIMULATIONS

Validation of the effectiveness of the combined model to capture streamflow was carried out. For this purpose, we compared the model results using measured rainfall and PE_A for 1980–2004 (the “original model”) with the model results from the downscaled rainfall and PE_S data for the same period (“validation model”). While it is not expected that the results from these two types of input will capture the exact annual sequence, we do expect that the overall interannual variability and daily cumulative distribution to be the same. We also expect the model to be able to capture the correct seasonality. To that end, we compare the cumulative distribution (from the maximal 100% to 99.5%, 97.5%, 90%, 75%, median 50%, and 25%, 10%, 2.5%, 0.5%–0%) of the predicted flows from the validation model with the flows from the original model (Fig. 13). According to this test ($R^2 > 0.99$ between fractions of both distributions), the model does a skillful job of representing the distribution of daily streamflows. The same results were achieved when we compared in similar way the flows of each of the three streams separately.

2) EFFECT OF SNOWMELT ON STREAMFLOW TIMING

In this section, the snow routine is tested in detail. It was found that in the higher elevations, there was a clear difference between the timing of effective precipitation (snowmelt + rainfall) compared to precipitation when snowmelt was not taken into account. Figure 14 shows the modeled contribution to the Jordan River streamflow during the wet season of 1991/92 from three altitude bands. This year was selected for Fig. 14 because it was an extremely cold winter, and the wettest season in the region since 1970. Therefore, it can exemplify clearly the snowmelt contribution to the streamflow. While using the model, we found that snow remained on top of the mountain into the middle of the summer, and that the calculated snowmelt contribution to both the fast flow and the base flow of the Jordan River were nearly insignificant. In Fig. 14a the effective precipitation (mm day^{-1}) for each altitude is presented. It should be noted that during October–December, temperatures were relatively high and no snow accumulation occurred. Moreover, precipitation during this period gradually saturated the upper soil layer and therefore very little flow to the streams occurred (Fig. 14b). During the spring months, snowmelt at 2025 and 2775 m altitude was high (Fig. 14a), but the contribution of these two high altitudes to the flow of the Jordan River ($1000 \text{ m}^3 \text{ day}^{-1}$; Fig. 14b) is minimal because of the

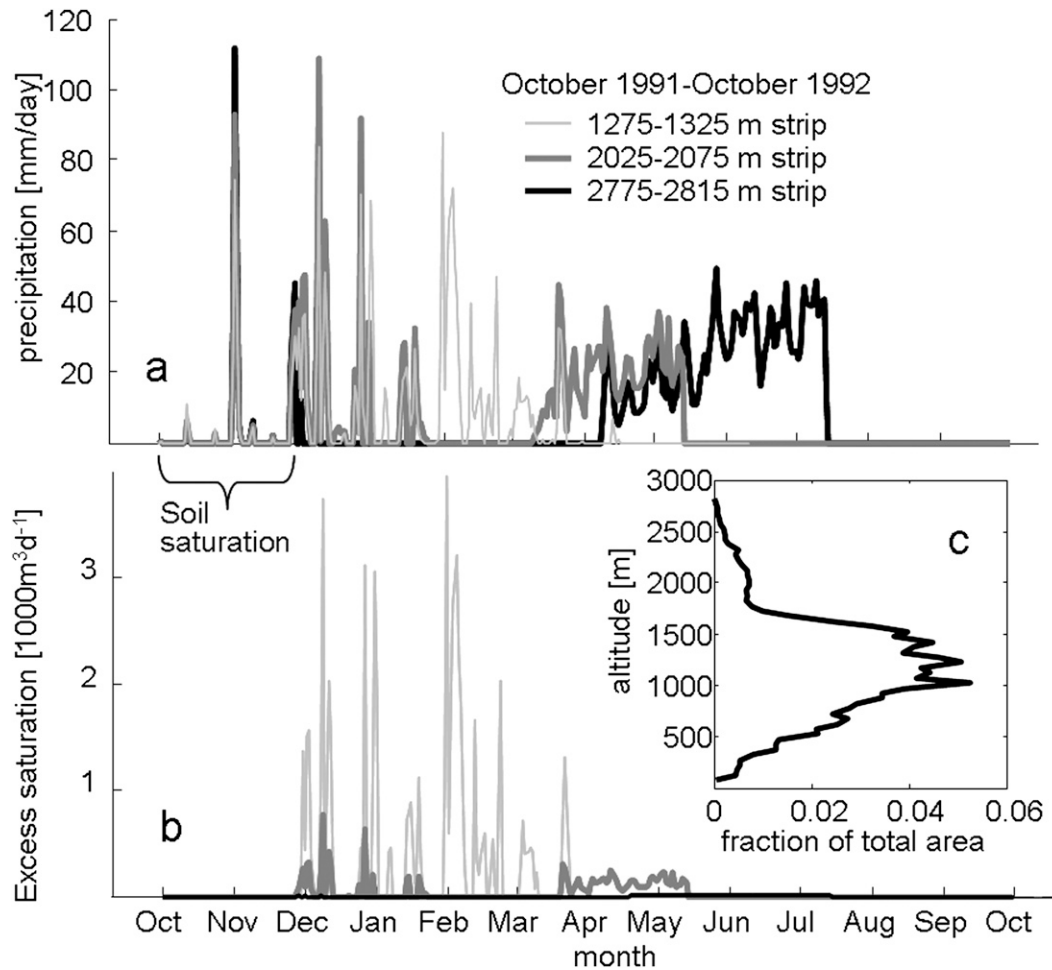


FIG. 14. Contribution of three altitude bands to the Jordan River streamflow during the extremely wet season of 1991/92. (a) Effective precipitation (snowmelt + rainfall) in each band (mm day^{-1}). During October–December, precipitation saturates the soil with very little flow to the streams. During the spring months, snowmelt at 2025 and 2775 m is high. (b) Excess saturation (1000 m^3) is the dominant contribution component of the surface layer to streamflow. The relative contribution of snowmelt from altitudes of 2025 and 2775 m is minimal because of the smaller area in these two bands. (c) Fraction of altitudes in the total area of Mount Hermon catchments.

physical area associated with these stripes (Fig. 14c). Therefore, the changes of form of precipitation and snowmelt had almost no effect on the final results of the daily streamflow. The effect of altitude area is also shown in Fig. 15, where we illustrate the average monthly difference between the contribution of the entire Mount Hermon catchment to the Jordan River streamflow, when it was calculated with and without the snow routine between 1970 and 2000. These differences are plotted as a percentage of the average annual precipitation on the entire Mount Hermon catchment. Each full bar in Fig. 15 represents the monthly difference between the amount of water contributed to the Jordan River without and with snow calculations. Each bar is composed of four altitude regions. The difference is usually positive during December–February

because during this period, part of the precipitation remains on the higher elevations as snow and does not contribute to streamflow. It is negative during March–June because during this period there is little rainfall, with most of the contribution to the streamflow coming from snowmelt at very high altitudes. However, these entire differences are at most $\pm 1\%$ of the flow in the Jordan River; therefore, they nearly went unnoticed in the streamflow results.

The following is a summary of our findings regarding the effect of snow and snowmelt.

1) The cumulative area of altitudes contributing snowmelt to the streamflow is less than 12% of the entire catchments area.

2) Because of the relatively high temperature and high solar radiation on Mount Hermon, temperature often

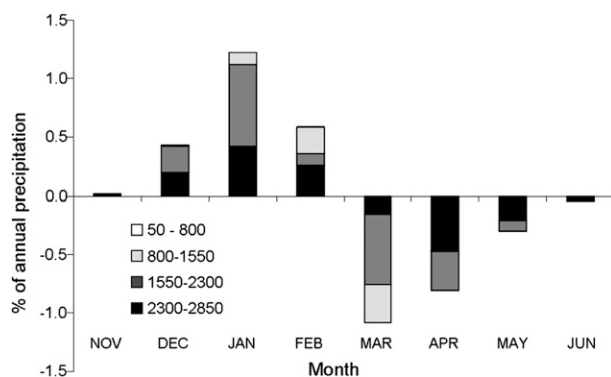


FIG. 15. The monthly difference between the contribution of four elevation bands ($50 < h < 800$; $800 < h < 1550$; $1550 < h < 2300$; $2300 < h < 2850$) with and without snow routine to the Jordan River streamflow, expressed as a percentage of the annual precipitation on the entire Mount Hermon catchments. Analysis is based on daily calculations between 1970 and 2000.

crosses the zero level during the winter, resulting in a continuous snowmelt process at almost all elevations; therefore, the delay in snowmelt application compared to the rainfall usually takes only few days.

3) Only at very high altitudes (>2000 m) is there a significant delay because of snowmelt (sometimes until April–June), but their contribution to streamflow is minimal because they have a very small area.

4) Since most of the river flow is from groundwater, there are several lagging mechanisms (surface wetness, vadose zone flow, and groundwater flow) that almost totally even out the effect of the surface precipitation, so that the only changes of streamflow are according to the effect of precipitation amount and not precipitation timing [Samuels et al. (2009) showed it in detail for the same hydrological catchments].

Taking into account that snowmelt has nearly no effect on the timing of the Jordan River streamflow, this aspect was not further tested in the future projections (see next subsection). It should, however, been taken into account if a model is used with shorter time intervals, and for other purposes than streamflow (skiing availability, surface fauna and flora, among others).

3) FUTURE PROJECTIONS

For future projections, we looked at streamflows during the validation period (1980–2005) together with the two future periods: near future (2010–35, “second” period) and far future (2036–60, “third” period). The RegCM3 projected only slight changes in precipitation and PE amounts during the second period but a more noticeable decrease of $\sim 10\%$ in mean annual rainfall amounts during the third period. Together with a small ($\sim 5\%$) mean annual increase in PE, these changes lead

to a comparable reduction in the streamflow. However, the hydrological response (and the model structure) is not linear by definition, and the reduction in streamflow is not necessarily similar in all sources, and not necessarily similar to the reduction in rainfall amounts. In this case, however, the 10% reduction in rainfall is well reflected by the 10%–11% reduction in daily mean base flow for all the rivers. For the Hermon, Snir, and Jordan, there is a 17% reduction in daily mean surface flow, indicating a nonlinear response system in this parameter.

Table 3 shows the distributions and moments of base flow and surface flow in the Dan, Hermon, Snir, and the Jordan River in the three tested periods. Figure 16 shows the distribution of the total flows (surface flow and base flow combined). For the Dan, there is an increase of more than 30% in standard deviation of daily base flow. For the Hermon and Snir, there is a decrease in standard deviation by 7% and 8% in daily base flow and 10% and 11% in daily surface flow, respectively. For the Jordan River, which is fed by the three rivers described, the mean daily base flow decreases by about 10% in the third period as compared with the first period while the standard deviation increases by 6%. The surface flow daily mean decreases by 17% with a decrease of 10% in standard deviation; however, since the flow is only about one-quarter of the base flow, this change is less significant than it seems.

Additionally, for both the Jordan River base flow, where most of the water flows, and for the Dan base flow, which contributes almost 60% of the Jordan base flow, there is an increase in the top 2.5% quantile as well as in the standard deviation. This indicates that even though there is a decrease in the total streamflow, there is increased variability and risk of extreme events.

6. Discussion and conclusions

We have presented a methodology for taking large-scale climate model results and reconciling them to the spatial scale necessary for hydrological and other response models. The results presented here, based on a single climate model, should be seen as a first approximation that can provide important information to planners and water managers but should be verified and compared with results from other climate models. The future trend described here, showing little change in precipitation in the earlier 2010–35 period with much of the decrease in precipitation taking place in the 2035–60 period, is consistent with the trends of the driving ECHAM GCM, which is characterized by a slower drying than most of the models from the 2020–40 period but catches up in the later decades (2040–60 and 2060–80;

TABLE 3. Distributions and moments of base flow and surface flow in the Dan, Hermon (Hrm), Snir (Snr), and the Jordan River (Jdn) in the three tested periods: 1) 1980–2005; 2) 2010–35; 3) 2036–60.

Distributions													
Base flow (1000 m ³ day ⁻¹)													
Quantiles	%	Dan 1	Dan 2	Dan 3	Hrm 1	Hrm 2	Hrm 3	Snr 1	Snr 2	Snr 3	Jdn 1	Jdn 2	Jdn 3
Maximum	100.0	1273.9	1363.7	1397.3	745.6	708.0	709.8	713.9	671.7	653.8	2336.7	2332.6	2527.7
	99.5	1083.0	1160.5	1254.4	669.8	664.0	645.6	622.2	618.8	588.1	2251.3	2285.0	2380.0
	97.5	1036.8	1107.0	1107.9	549.8	572.7	514.9	504.0	531.4	468.0	1958.0	2029.9	1971.9
	90.0	910.3	973.0	862.2	428.5	442.9	386.3	380.8	391.7	336.7	1609.8	1688.7	1479.7
Quartile	75.0	790.8	864.8	733.7	302.5	307.9	271.0	252.9	259.8	224.7	1303.5	1368.3	1203.2
Median	50.0	702.1	714.4	610.0	201.3	196.2	177.7	155.2	151.6	133.0	1050.8	1081.2	926.6
Quartile	25.0	611.7	606.6	517.2	134.2	132.5	117.9	95.4	94.8	83.0	861.6	866.6	743.6
	10.0	541.2	540.7	422.2	108.3	107.2	100.0	75.3	73.9	68.8	743.4	736.4	611.3
	2.5	463.6	454.5	325.7	93.9	91.1	85.1	64.8	62.2	57.1	625.0	611.5	489.9
Minimum	0.5	407.2	410.2	268.7	83.6	83.6	72.8	54.5	57.1	48.8	559.7	557.4	388.7
	0.0	384.4	393.6	256.9	77.9	80.9	70.1	51.7	54.7	47.1	532.2	535.2	376.9
Moments													
Mean		711.4	739.8	637.0	237.0	239.5	213.0	193.7	196.6	171.7	1117.5	1150.5	1001.5
Std dev		142.5	167.4	188.3	128.5	135.5	119.4	124.0	130.3	113.8	342.1	373.3	363.6
Std err mean		1.5	1.8	2.0	1.3	1.4	1.2	1.3	1.4	1.2	3.6	3.9	3.8
Upper 95% mean		714.3	743.2	640.9	239.6	242.3	215.4	196.2	199.3	174.1	1124.5	1158.2	1008.9
Lower 95% mean		708.4	736.4	633.2	234.4	236.7	210.5	191.2	193.9	169.4	1110.5	1142.8	994.0
<i>N</i>		9132	9131	9132	9132	9131	9132	9132	9131	9132	9132	9131	9132
Distributions													
Surface flow (1000 m ³ day ⁻¹)													
Quantiles	%	Dan 1	Dan 2	Dan 3	Hrm 1	Hrm 2	Hrm 3	Snr 1	Snr 2	Snr 3	Jdn 1	Jdn 2	Jdn 3
Maximum	100.0				1866.0	2089.0	1881.7	3745.0	3867.0	3450.7	6228.9	6589.9	5955.4
	99.5				1150.9	1183.2	1059.5	2073.3	2150.0	1941.5	3613.5	3697.9	3324.1
	97.5				668.3	699.7	595.2	1173.2	1248.9	1066.8	2046.8	2165.8	1861.8
	90.0				264.2	265.7	218.5	416.9	419.3	324.2	764.3	773.0	616.9
Quartile	75.0				27.6	26.9	9.6	25.0	24.5	6.4	62.3	60.7	19.4
Median to minimum	50.0 to 0.0				No flow								
Moments													
Mean					74.2	76.7	61.4	121.5	125.7	100.6	220.2	227.9	182.3
Std dev					189.0	197.7	168.8	334.2	350.0	300.3	584.8	612.1	524.0
Std err mean					2.0	2.1	1.8	3.5	3.7	3.1	6.1	6.4	5.5
Upper 95% mean					78.0	80.8	64.8	128.4	132.9	106.8	232.2	240.4	193.0
Lower 95% mean					70.3	72.7	57.9	114.7	118.6	94.4	208.2	215.3	171.5
<i>N</i>					9132	9131	9132	9132	9131	9132	9132	9131	9132

Parry et al. 2007). This trend can be identified in our model results here by the little changes during the earlier 2010–35 period, with much of the decrease in precipitation taking place in the 2035–60 period.

One important aspect that we investigated was the effect of changes in snowmelt on the streamflow. Little work has been done on snow dynamics in warm regions located in low latitudes (<40°N), where snow is only ephemeral. Snow at low latitudes can be important, especially on high mountains. In the Atlas Mountains, snow is a significant water source to the lowlands of southeastern Morocco (Boulet et al. 2009; Schulz and de Jong 2004). Aouad-Rizk et al. (2005) reported that in Mount Lebanon, up to 40% of annual precipitation is stored as snow during spring and summer. In Mount Hermon, the subject of the current study, Gil'ad and

Bonne (1990) concluded that snow storage accounts for ~10% of the Jordan River annual yields. The main snow feature in warm climate is rapid changes in snow cover, and several complete melting cycles may occur during one winter season (Herrero et al. 2009). The aspect that we concentrated on—how changes in snowmelt are expected to affect streamflow—was proven to be nearly insignificant, mainly because of the small contributing area of snowmelt. However, it is emphasized here that our conclusions regarding the importance of the snow cover to the Jordan River flow are a result of a basic study, and more research is needed to comprehend the full hydrological mechanism.

The entire analysis was based on the expected future meteorological changes. While this is necessary as a start, it is incomplete in terms of providing the whole

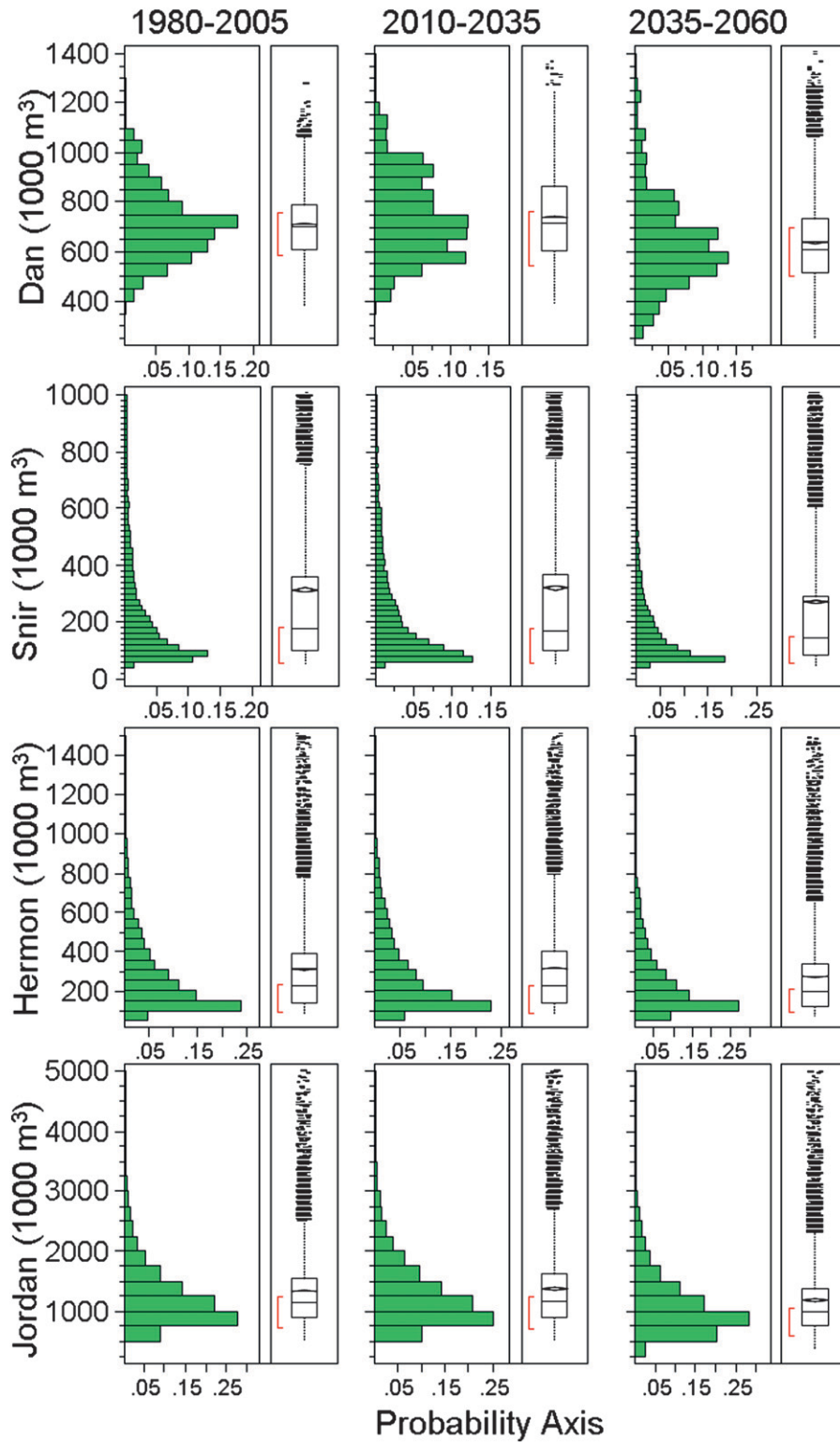


FIG. 16. Distribution of flow in the Dan, Snir, Hermon streams, and the Jordan River in the three tested periods 1980–2005, 2010–35, and 2036–60.

picture of the future hydrological cycle. For example, the direct CO₂ effects on evaporation due to long-term changes in vegetation were not taken into account. Given the seasonality of rainfall with dry summers and wet winters, it is not expected that these effects will play a major role in this region. Other aspects that were not taken into account are the effects of land use changes; however, Mount Hermon catchments are relatively unchanged in terms of land use because of the sharp mountainous ground surface.

Integration between the different models is necessary to obtain reliable information about the effect of climate change at the local level. Previous models have used output from GCMs and RCMs to calculate evaporation (e.g., Baguis 2010; Kay and Davies 2008; Rotstayn et al. 2006). However, these studies calculate the evaporation based on monthly means, whereas here we calculate it on a daily basis for the purpose of daily streamflow analysis. The case study of the Jordan River provides an example of how climate model results can be directly input into a hydrological impact model that can be used to inform the decision-making process. We show that based on this simulation, the changes in streamflow of the Jordan River and its tributaries are not significant in the near future; however, in the far future, a reduction in streamflow is expected along with an increase in peak base flow and variability. This has implications for water planning and management.

We have demonstrated the results of the first implementation of a methodology that may be used for climate change risk assessment in the EM region. While here the methodology is applied to a single climate model simulation, the application to multiple models would create a method for obtaining a highly skillful “climate-informed risk assessment,” a tool that is becoming more and more crucial in a variable and evolving environment.

Acknowledgments. We thank Pavel Kunin and Netta Tsur for preparing daily time series based on results of the RegCM3 climate simulation experiment. We would also like to thank Daniel Yekutieli for his insights into the statistical aspects of bias correction. We thank Mop Zafon for their excellent Web site. We also thank Moshe Meron and Joseph Tsipris for their support with the meteorological data from the Agrometeorology Services of the Upper Galilee Regional Council. The comments of three anonymous reviewers have helped us to greatly improve this manuscript. This research was partly supported by GLOWA Jordan River Project, funded by the German Federal Ministry of Education and Research (BMBF) in collaboration with the Israeli Ministry of Science and Technology (MOST).

REFERENCES

- Allen, R. G., L. S. Pereira, D. Raes, and M. Smith, 1998: Crop evapotranspiration: Guidelines for computing crop water requirements. FAO Irrigation and Drainage Paper 56, 300 pp.
- Alpert, P., S. O. Krichak, H. Shafir, D. Haim, and I. Osetinsky, 2008: Climatic trends to extremes: Employing regional modeling and statistical interpretation over the E. Mediterranean. *Global Planet. Change*, **63**, 163–170.
- Aouad-Rizk, A., J.-O. Job, S. Khalil, T. Touma, C. Bitar, C. Bocquillon, and W. Najem, 2005: Snow in Lebanon: A preliminary study of snow cover over Mount Lebanon and a simple snowmelt model. *Hydrol. Sci. J.*, **50**, 555–569.
- Arakawa, A., and W. Schubert, 1974: Interaction of a cumulus cloud ensemble with the large-scale environment, Part I. *J. Atmos. Sci.*, **31**, 674–701.
- Baguis, P., 2010: Climate change scenarios for precipitation and potential evapotranspiration over central Belgium. *Theor. Appl. Climatol.*, **99**, 273–286.
- Bergström, S., 1995: The HBV model. *Computer Models of Watershed Hydrology*, V. P. Singh, Ed., Water Resources Publications, 1130 pp.
- Boulet, G., A. Boudhar, L. Hanich, B. Duchemin, G. Chehbouni, and B. Berjamy, 2009: Impact of the snow cover estimation method on the Snowmelt Runoff Model performance in the Moroccan High Atlas Mountains. *Geophysical Research Abstracts*, Vol. 11, Abstract EGU2009-6590. [Available online at <http://meetingorganizer.copernicus.org/EGU2009/EGU2009-6590.pdf>.]
- Buishand, T. A., and T. Brandsma, 2001: Multisite simulation of daily precipitation and temperature in the Rhine basin by nearest-neighbor resampling. *Water Resour. Res.*, **37**, 2761–2776.
- Davies, H., and R. Turner, 1977: Updating prediction models by dynamical relaxation: An examination of the technique. *Quart. J. Roy. Meteor. Soc.*, **103**, 225–245.
- Déqué, M., 2007: Frequency of precipitation and temperature extremes over France in an anthropogenic scenario: Model results and statistical correction according to observed values. *Global Planet. Change*, **57**, 16–26.
- Dickinson, R., A. Henderson-Sellers, and P. J. Kennedy, 1993: Biosphere–Atmosphere Transfer Scheme (BATS) version 1E as coupled to the NCAR community climate model. NCAR Tech. Note NCAR/TN-387+STR, 85 pp.
- Díez, E., C. Primo, J. A. García-Moya, J. M. Gutiérrez, and B. Orfila, 2005: Statistical and dynamical downscaling of precipitation over Spain from DEMETER seasonal forecasts. *Tellus*, **57A**, 409–423.
- Eckhardt, K., 2005: How to Construct Recursive Digital Filters for Baseflow Separation. *Hydrol. Processes*, **19**, 507–515.
- Elguindi, N., B. Xunqiang, F. Giorgi, B. Nagarajan, J. Pal, F. Solmon, S. Rauscher, and A. Zakey, 2007: RegCM version 3.1 user’s guide. Abdus Salam ICTP, 57 pp.
- Fowler, H. J., and M. Ekström, 2009: Multi-model ensemble estimates of climate change impacts on UK seasonal rainfall extremes. *Int. J. Climatol.*, **29**, 385–416.
- Fritsch, J., and C. Chappell, 1980: Numerical prediction of convectively driven mesoscale pressure systems. Part I: Convective parameterization. *J. Atmos. Sci.*, **37**, 1722–1733.
- Gao, X., J. Pal, and F. Giorgi, 2006: Projected changes in mean and extreme precipitation over the Mediterranean region from a high resolution double nested RCM simulation. *Geophys. Res. Lett.*, **33**, L03706, doi:10.1029/2005GL024954.

- Gil'ad, D., and J. A. Bonne, 1990: The snowmelt of Mt. Hermon and its contribution to the sources of the Jordan River. *J. Hydrol.*, **114**, 1–15.
- Giorgi, F., X. Bi, and J. Pal, 2004: Mean, interannual variability and trends in a regional climate change experiment over Europe. II. Climate change scenarios (2071–2100). *Climate Dyn.*, **23**, 839–858.
- Grell, G., 1993: Prognostic evaluation of assumptions used by cumulus parameterizations. *Mon. Wea. Rev.*, **121**, 764–787.
- Hamilton, A. S., D. G. Hutchinson, and R. D. Moore, 2000: Estimating winter streamflow using conceptual streamflow model. *J. Cold Reg. Eng.*, **14**, 158–175.
- Herrero, J., M. J. Polo, A. Moñino, and M. A. Losada, 2009: An energy balance snowmelt model in a Mediterranean site. *J. Hydrol.*, **371**, 98–107.
- Holtlag, A. A. M., E. I. F. de Bruijn, and H.-L. Pan, 1990: A high resolution air mass transformation model for short-range weather forecasting. *Mon. Wea. Rev.*, **118**, 1561–1575.
- Kay, A. L., and H. N. Davies, 2008: Calculating potential evaporation from climate model data: A source of uncertainty for hydrological climate change impacts. *J. Hydrol.*, **358**, 221–239.
- Kiehl, J., J. Hack, G. Bonan, B. Boville, B. Briegleb, D. Williamson, and P. Rasch, 1996: Description of the NCAR Community Climate Model (CCM3). NCAR Tech. Note TN-420+STR, 152 pp.
- Kim, M.-K., I.-S. Kang, C.-K. Park, and K.-M. Kim, 2004: Superensemble Prediction of Regional Precipitation over Korea. *Int. J. Climatol.*, **24**, 777–790.
- Krichak, S., P. Alpert, K. Bassat, and P. Kunin, 2007: The surface climatology of the eastern Mediterranean region obtained in a three-member ensemble climate change simulation experiment. *Adv. Geosci.*, **12**, 67–80.
- , —, and P. Kunin, 2009: Projections of climate change over non-boreal East Europe during first half of XXI century according to results of a transient RCM experiment. *Regional Aspects of Climate-Terrestrial-Hydrologic Interactions in Non-boreal Eastern Europe*, P. Ya. Groisman and S. V. Ivanov, Eds., Springer, 55–62.
- Kunstmann, H., P. Suppan, A. Heckl, and Rimmer, 2007: Regional climate change in the Middle East and impact on hydrology in the Upper Jordan catchment. *Quantification and Reduction of Predictive Uncertainty for Sustainable Water Resources Management*, E. Boegh et al., Eds., IAHS Publ. 313, IAHS, 141–149.
- Lloyd-Hughes, B., and M. A. Saunders, 2002: Seasonal prediction of European spring precipitation from El Niño-Southern Oscillation and Local sea-surface temperatures. *Int. J. Climatol.*, **22**, 1–14.
- Moore, R. D., 1993: Application of a conceptual streamflow model in a glacierized drainage basin. *J. Hydrol.*, **150**, 151–168.
- Pal, J. S., and Coauthors, 2007: Regional climate modeling for the developing world: The ICTP RegCM3 and RegCNET. *Bull. Amer. Meteor. Soc.*, **88**, 1395–1409.
- Parry, M. L., O. F. Canziani, J. P. Palutikof, P. J. van der Linden, and C. E. Hanson, Eds., 2007: *Climate Change 2007: Impacts, Adaptation and Vulnerability*. Cambridge University Press, 976 pp.
- Pierce, D. W., T. P. Barnett, B. D. Santer, and P. J. Gleckler, 2009: Selecting global climate models for regional climate change studies. *Proc. Natl. Acad. Sci. USA*, **106**, 8441–8446.
- Ponce, V. M., 1989: *Engineering Hydrology: Principles and Practices*. Prentice Hall, 640 pp.
- Rimmer, A., 2008: Hydrological models to support water policy: The case of Lake Kinneret watershed, Israel. *Managing Water Resources in Time of Global Change: Mountains, Valleys and Flood Plains*, A. Dinar and A. Garrido, Eds., Routledge, 50–66.
- , and Y. Salingar, 2006: Modelling precipitation-streamflow processes in karst basin: The case of the Jordan River sources, Israel. *J. Hydrol.*, **331**, 524–542.
- Robertson, A. W., S. Kirshner, and P. Smyth, 2004: Downscaling of daily rainfall occurrence over northeast Brazil using a hidden Markov model. *J. Climate*, **17**, 4407–4424.
- Roeckner, E., and Coauthors, 2003: The atmospheric general circulation model ECHAM5, Part I: Model description. Max Planck Institute for Meteorology Rep. 349, 140 pp. [Available from MPI for Meteorology, Bundesstr. 153, 20146 Hamburg, Germany.]
- Rotstayn, L. D., M. L. Roderick, and G. D. Farquhar, 2006: A simple pan-evaporation model for analysis of climate simulations: Evaluation over Australia. *Geophys. Res. Lett.*, **33**, L17715, doi:10.1029/2006GL027114.
- Samuels, R., 2008: Understanding and predicting climate variations in the Middle East for sustainable water resource management and development. Ph.D. dissertation, Columbia University, 218 pp.
- , A. Rimmer, and P. Alpert, 2009: Effect of Extreme Rainfall Events on the Water Resources of the Jordan River, Israel. *J. Hydrol.*, **375**, 513–523.
- Schulz, O., and C. de Jong, 2004: Snowmelt and sublimation: Field experiments and modeling in the High Atlas Mountains of Morocco. *Hydrol. Earth Syst. Sci.*, **8**, 1076–1089.
- Seibert, J., 1997: HBV light 1.2, user's manual. Department of Earth Sciences, Hydrology, Uppsala University, 32 pp.
- Tath, H., H. N. Dalfes, and S. S. Montes, 2004: A Statistical Downscaling Method for Monthly Total Precipitation over Turkey. *Int. J. Climatol.*, **24**, 161–180.
- Valiantzas, J. D., 2006: Simplified versions for the Penman evaporation equation using routine weather data. *J. Hydrol.*, **331**, 690–702.
- Vicuna, S., and J. A. Dracup, 2007: The evolution of climate change impact studies on hydrology and water resources in California. *Climatic Change*, **82**, 327–350.
- Viney, N. R., and M. Sivapalan, 1996: The hydrological response of catchments to simulated changes in climate. *Ecol. Modell.*, **86**, 189–193.
- Zeng, X., M. Zhao, and R. E. Dickinson, 1998: Intercomparison of bulk aerodynamic algorithms for the computation of sea surface fluxes using TOGA COARE and TAO data. *J. Climate*, **11**, 2628–2644.